Available online at www.sciencedirect.com

ScienceDirect

Proceedings of the Combustion Institute 35 (2015) 2241–2248

Proceedings of the Combustion Institute

www.elsevier.com/locate/proci

Characterization of the NO-soot combustion process over $La_{0.8}Ce_{0.2}Mn_{0.7}Bi_{0.3}O_3$ catalyst

Feng Bin [a,b], Chonglin Song [a,*], Gang Lv [a], Xiaodong Li [a], Xiaofeng Cao [a,b], Jinou Song [a], Shaohua Wu [a]

[a] State Key Laboratory of Engines, Tianjin University, Tianjin 300072, PR China
[b] State Key Laboratory of High-Temperature Gas Dynamics, Institute of Mechanics, Chinese Academy of Science, Beijing 100190, PR China

Available online 13 September 2014

Abstract

The combustion of diesel soot in $NO + O_2$/He atmospheres was investigated by temperature-programmed oxidation (TPO), X-ray photoelectron spectroscopy (XPS), and in-situ diffuse reflectance Fourier transform (DRIFT) technology, with the aim to demonstrate the participation of nitric oxide species and surface carbon-oxygenated complexes in the process. According to the TPO results, two main adsorption periods for nitric oxide species were observed: one was from 50 to about 180 °C and the other occurred in the temperature range of 180–400 °C. The DRIFT results indicated that the first adsorption period was mainly associated with weakly adsorbed NO, bidentate nitrite and unidentate nitrate, monodentate nitrate, chelating nitrate and bridging nitrate, while the second uptake was related to nitrite and free nitrate species. Based on the XPS and DRIFT results, possible reaction processes for the NO_x-soot combustion are proposed based on the Langmuir–Hinshelwood mechanism. First, the carbon-oxygenated groups, including carboxyls, lactones, and anhydrides were formed at free carbon sites by the oxidation of dissociative nitrates. Such moieties were so stable that they could not be further oxidized, even at 400 °C, without the presence of a catalyst. Second, the adsorption of $NO + O_2$ resulted in the formation of nitrates on the MnO_x surface of the catalyst. Then, the surface-activated nitrates, with activity decreasing in the order: chelating nitrates > bridging nitrates > monodentate nitrates > free ionic nitrates, further oxidized these carbon-oxygenated complexes with subsequent release of CO_2, NO and N_2.

Keywords: Soot; Nitrous oxide; Catalytic combustion; Perovskite catalyst

1. Introduction

The diesel particle filter combined with catalytic combustion technology appears to be the most practical method to eliminate soot from diesel exhaust emissions. Catalytic combustion of soot in the presence of NO, so-called CRT (continuously regenerating trap) technology, generally involves two steps. First, the NO is oxidized to NO_2 over catalysts, and then the NO_2, as a strong oxidizer, is used to continuously oxidize the soot collected on the filter at a temperature much lower

* Corresponding author. Fax: +86 22 27403750.
E-mail address: songchonglin@tju.edu.cn (C. Song).

http://dx.doi.org/10.1016/j.proci.2014.08.028
1540-7489/

than that required with either NO or O_2. To promote the $NO \rightarrow NO_2$ conversion and lower the soot combustion temperature, development work has been undertaken on several catalysts, such as noble metals [1], transition metal oxides [2], alkaline metal oxides [3], perovskite oxides [4], and ceria-based oxides [5].

For real application, it is necessary to have a better understanding of the NO_x–O_2-soot reaction mechanism to improve emission control, minimize fuel consumption, and maximize catalyst efficiency. Shuangguan et al. [6] supposed that the NO_2 formed in the gaseous phase is adsorbed dissociatively on the catalyst surface as NO_{ad} and O_{ad}. Then, the NO_{ad} species react with surface carbon complexes $C^*[N,O]$ to produce CO_2 and N_2. Tschamber et al. [1] proposed a mechanism featuring two routes: a direct reaction with gaseous NO_2 attacking carbon and a route with NO_2 undergoing adsorption on $C^*[O]$ complexes to form nitro-oxygenated intermediate species, which are then decomposed by NO_2. Although these mechanisms provide a good starting point for investigating the NO_x–O_2-soot reaction, there are no reports on the actual state of the adsorbed NO_x and the formation pathway(s) of NO_2 under in-situ reaction conditions.

Recently, López–Suárez et al. [7] demonstrated, in accordance with in-situ diffuse reflectance Fourier transform (DRIFT) data, that the monodentate, chelating, and bridging nitrites together with the corresponding nitrates are formed on the metal sites when the $Cu/SrTiO_3$ sample is exposed to a $NO + O_2$ mixture. Pieta et al. [8] found that prolonged exposure of Pt–Ba catalysts to $NO + O_2$ or an increase in reaction temperature led to the decomposition of nitrites with the formation of the corresponding nitrates. According to Wu et al. [9], both the nitrates formed by adsorption of NO on the catalyst and the NO_2 released from decomposition of surface nitrates is of importance for soot oxidation. However, little information is available on the contribution of nitrates to the soot combustion.

Although CRT technology has been employed on a commercial scale, it has some drawbacks owing to system complexity and the potential adverse environmental impact of excessive NO_2 exhaust emissions. Recently, we have developed an innovative $La_{0.8}Ce_{0.2}Mn_{0.7}Bi_{0.3}O_3$ catalyst, which can facilitate the NO-soot reaction and promote combustion of soot at 330 °C in a NO/O_2/He atmosphere. In the present study, we address the NO-soot combustion process over this catalyst. In the presence of $NO + O_2$, the effects of both nitrates and surface carbon-oxygenated complexes on the soot combustion process have been investigated, and potential reaction mechanisms are discussed in detail.

2. Experimental section

2.1. Synthesis of catalysts

The $La_{0.8}Ce_{0.2}Mn_{0.7}Bi_{0.3}O_3$ perovskite oxide was synthesized according to the citric acid method. Briefly, the manganese acetate, lanthanum, cerium, and bismuth nitrate salts in the desired stoichiometric ratio were dissolved in deionized water. Citric acid monohydrate was then added in 100 wt% excess to ensure metal ion complexation. The resulting solution was evaporated to dryness at 90 °C with vigorous stirring until the spongy material was formed. The obtained precursor was calcined at 800 °C for 4 h. Catalyst chemical composition was tested by inductively coupled plasma-atomic emission spectroscopy to verify that experimental values were in agreement with theoretical values.

2.2. Temperature-programmed oxidation

Temperature-programmed oxidation (TPO) was performed on a ChemBet Pulsar system to investigate NO_x adsorption, desorption, and reduction over the catalyst. The substitute for diesel soot in this experiment was a model carbon particle (Printex-U, Degussa AG). This model soot consisted mainly of 5.2 wt% hydrocarbons, < 0.1 wt% ash, 92.2 wt% C, 0.6 wt% H, 0.2 wt% N, and 0.4 wt% S, and its properties were similar to those of real diesel particulate soot [10]. TEM image of this soot was obtained using an HRTEM (Philips Tecnai F20) with a point resolution of 0.248 nm operating at 200 kV. The TEM image in Fig. 1 showed that the Printex-U soot was present as spherical particles with the diameters of 25–35 nm. The catalyst (180 mg) and model soot (20 mg) were mixed with a spatula, and then packed between two quartz wool plugs in the center of a cylindrical quartz tube reactor (6-mm internal diameter). The quartz reactor was mounted in a tube furnace and the reaction temperature was controlled through a PID-regu-

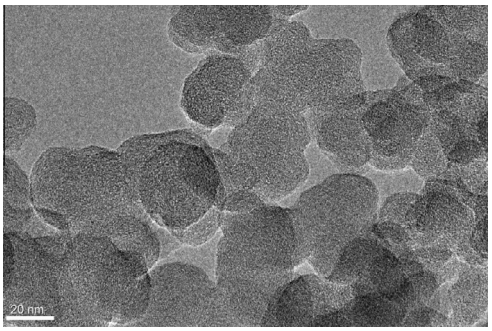

Fig. 1. TEM image of Printex-U soot used as the model soot.

lation system based on the measurements of a K-type thermocouple inserted in the center of the catalyst/soot mixture. A feed gas, containing 500 ppm NO + 10 vol.% O_2, was employed with He as the balance gas. Due to the occurrence of thermal runaway at the gas flow rate of 50 mL/min, the gas flow rate was set to 30 mL/min. During each TPO run, the reaction temperature range was 50–600 °C with a heating rate of 2 °C/min. An online mass spectrometer (Dycor LC-D200; AMETEK) was used to monitor the effluent gases, CO, CO_2, N_2, and NO_x.

To evaluate the NO_x yielded from the nitrogen element in the model soot, a TPO run was performed under the identical operation condition mentioned above. The feed gas used is 10 vol.% O_2 with He as the balance gas. The peak value of releasing NO_x is found below 8 ppm in the temperature range of 200–600 °C. Therefore, the NO_x yielded from the model soot is ignorable when compared with the 500 ppm NO in 30 mL/min gas.

2.3. XRD, XPS, and in-situ DRIFT analysis

The crystalline phase of each sample was determined by powder X-ray diffraction (XRD) using a Rigaku D/MAC/max 2500v/pc diffractometer with Cu Kα radiation (40 kV, 200 mA, $\lambda = 1.5418$ Å). X-ray photoelectron spectra (XPS) were recorded on a Perkin–Elmer PHI-1600 ESCA spectrometer using an Mg Kα X-ray source. In-situ diffuse reflectance Fourier transform (DRIFT) measurements were performed on a Bruker V70 FTIR spectrometer equipped with a mercury cadmium telluride detector. For the DRIFT test, a mixture with a catalyst/soot ratio of 10:1 by weight was made, and this catalyst/soot mixture was then mixed with KBr at a ratio of 1:20 by weight. When soot or catalyst alone was tested, the sample would still be diluted with KBr at the same weight ratio of 1:20. The samples in the DRIFT cell were purged in-situ by an Ar stream at 400 °C for 30 min, and then cooled to the desired temperature to record a reference spectrum. The DRIFT spectra for reactions on the sample were sequentially recorded with a resolution of 4 cm^{-1} and an accumulation of 64 scans.

3. Results and discussion

3.1. NO_x adsorption, desorption, and reduction during TPO

Figure 2 illustrates the profiles for the NO_x concentrations over the $La_{0.8}Ce_{0.2}Mn_{0.7}Bi_{0.3}O_3$ catalyst mixed with and without soot during TPO in atmospheres of NO + O_2/He. Herein, the dash dotted line represents the NO_x concentration in the gas feed, and the points below and above this

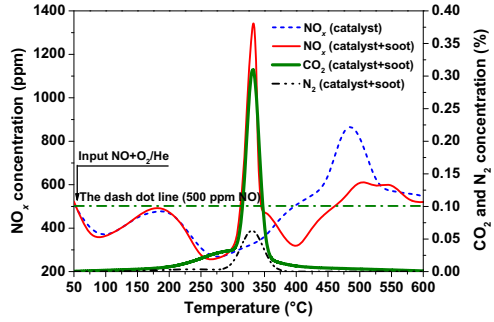

Fig. 2. Profiles of NO_x adsorption, desorption, and reduction in a NO + O_2/He atmosphere for the $La_{0.8}Ce_{0.2}Mn_{0.7}Bi_{0.3}O_3$ catalyst with or without soot.

line imply the occurrence of NO_x adsorption or reduction and NO_x desorption, respectively. For the $La_{0.8}Ce_{0.2}Mn_{0.7}Bi_{0.3}O_3$ catalyst alone, two main adsorption periods can be observed: the first being from 50 to about 180 °C and the other from 180 to 400 °C. At higher temperatures (>400 °C), the NO_x concentration becomes higher than that in the feed, which is the result of decomposition of adsorbed NO_x species.

The $La_{0.8}Ce_{0.2}Mn_{0.7}Bi_{0.3}O_3$ catalyst/soot mixture has a similar NO_x uptake profile as the $La_{0.8}Ce_{0.2}Mn_{0.7}Bi_{0.3}O_3$ catalyst alone in the temperature region 50 to 300 °C. As the temperature reaches 300 °C, however, a sharp desorption/reduction peak for the NO_x species is induced by the exotherm of soot combustion, which is followed by a clear decrease of NO_x concentration down to the dash dotted line below. From 367 to 532 °C, the NO_x concentration for the $La_{0.8}Ce_{0.2}Mn_{0.7}Bi_{0.3}O_3$ catalyst/soot mixture is lower than that for the $La_{0.8}Ce_{0.2}Mn_{0.7}Bi_{0.3}O_3$ catalyst alone, because of NO_x re-adsorption after soot combustion. Both CO_2 and N_2 are formed at the same time as the major products (see Fig. 2), which is wholly consistent with a simultaneous removal of NO_x and soot. The concentration of CO is below 10 ppm during soot oxidation (not shown). The formation of CO_2 occurs by a two-step process. The CO_2 induction process begins at 200 °C and then continues at a relatively slow rate, until about 300 °C. For the temperature range of 300–400 °C, the rate is similar to that for the release of NO_x, with a maximum soot combustion rate temperature of 332 °C.

3.2. In-situ NO + O_2 adsorption on $La_{0.8}Ce_{0.2}Mn_{0.7}Bi_{0.3}O_3$

Figure 2 shows the sorption of NO over $La_{0.8}Ce_{0.2}Mn_{0.7}Bi_{0.3}O_3$ alone, and the process consists of two steps in the temperature regions of 50–200 °C and 200–400 °C, respectively. To obtain information on the interaction of NO + O_2 with

the surface of the catalyst, in situ DRIFT experiments were performed, where the gas mixtures (0.5% NO + 10% O_2 or 10% O_2; He as balance) were fed at a flow rate of 50 mL/min. Due to the darkness of the soot, the flow rate fixed in the DRIFT experiments (50 mL/min) was higher than that in the TPO (30 mL/min) in order to the legible spectra. For the DRIFT experiments, no apparent difference in peak locations (wavenumbers) was observed at these two flow rates. The spectra were recorded from 100 to 400 °C at a heating rate of 10 °C/min. As shown in Fig. 3, the bands at 834 and 1003 cm^{-1} can be assigned to nitrite and unidentate nitrates, respectively [11]. The bands at 1275 cm^{-1} corresponds to bidentate nitrite species, and the band at 1349 cm^{-1} is attributable to free ionic nitrate [12]. Part of the NO adsorbed on the surface transition metal species exists as monodentate, chelating, and bridging nitrates, as denoted by absorptions at 1530, 1592, and 1630 cm^{-1}, respectively [13]. At higher wavenumbers, the bands at 1853 and 1905 cm^{-1} are caused by weakly adsorbed NO [14].

During the first uptake and storage of NO (50–200 °C), it is likely that multiple sites for NO_x adsorption are associated with various forms of nitrate/nitrite species, which form on the surface of the catalyst, and can be characterized as unidentate nitrate (1003 cm^{-1}), bidentate nitrite (1275 cm^{-1}), monodentate nitrate (1530 cm^{-1}), chelating nitrate (1592 cm^{-1}), and bridging nitrate (1630 cm^{-1}), as well as weakly adsorbed NO (1853 and 1905 cm^{-1}). As shown in Fig. 4, these speculations depend on the intensities of the bands at 1003, 1275, 1349, 1530, 1592, and 1630 cm^{-1}, which decrease with increasing temperature from 50 to 350 °C. Moreover, the bands at 1853 and 1905 cm^{-1} remain unchanged with an increase in temperature. In the second stage (200–400 °C), NO_x is probably stored as nitrite (834 cm^{-1}) and free ionic nitrate (1349 cm^{-1}). For the band at

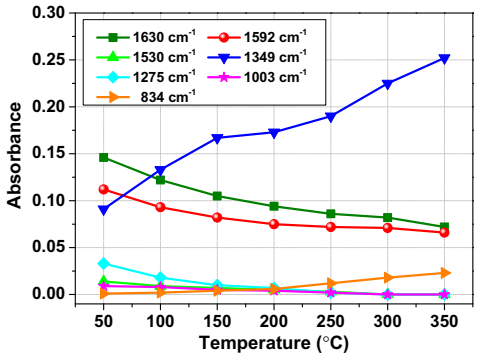

Fig. 4. Absorbance intensity variation of NO_x species with the increase of temperatures.

834 cm^{-1}, the clear increase of intensity can be observed at temperatures > 200 °C. For the band at 1349 cm^{-1}, the yield of free ionic nitrates occurs in a two-step process, i.e., from 50 to 150 °C and from 200 to 350 °C. Moreover, with an increase in temperature, the band at 1349 cm^{-1} predominates, presumably because of the strong oxidative capability of the catalyst.

3.3. Reaction of NO_x with soot on the surface of $La_{0.8}Ce_{0.2}Mn_{0.7}Bi_{0.3}O_3$

In-situ DRIFT technology was also employed to investigate the reaction between NO_x and soot over the $La_{0.8}Ce_{0.2}Mn_{0.7}Bi_{0.3}O_3$ catalyst. Herein, the catalyst/soot/KBr mixture was heated to 350 °C, and then a gas mixture of 0.5% NO + 10% O_2/He was passed at a flow rate of 50 mL/min. At the same time, spectra were recorded in succession at 2-min intervals. The reaction temperature, set at 350 °C, was close to the maximum combustion temperature of soot in the TPO process (Fig. 2). As shown in Fig. 5,

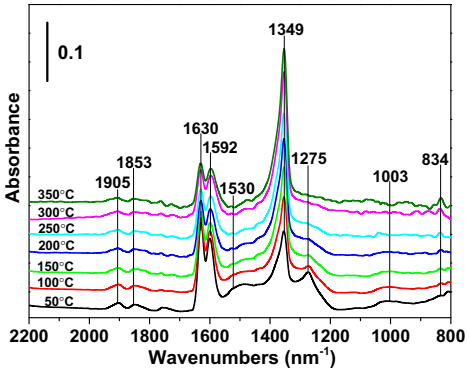

Fig. 3. DRIFT spectra for the $La_{0.8}Ce_{0.2}Mn_{0.7}Bi_{0.3}O_3$ catalyst alone and exposed to NO + O_2/He at different temperatures.

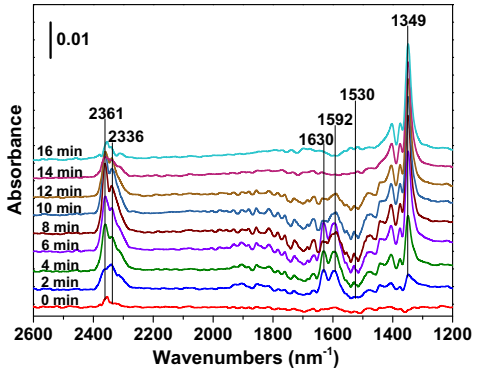

Fig. 5. DRIFT spectra recorded for the $La_{0.8}Ce_{0.2}Mn_{0.7}Bi_{0.3}O_3$ catalyst/soot mixture exposed to NO + O_2/He at 350 °C.

when the catalyst/soot mixture is exposed to the gas mixture containing $NO + O_2$, four bands attributable to adsorbed NO_x species with wave numbers at 1630 cm^{-1} (bridging nitrates), 1592 cm^{-1} (chelating nitrates), 1530 cm^{-1} (monodentate nitrates), and 1349 cm^{-1} (free ionic nitrates) are identified. In Fig. 6, the intensities for the bridging, chelating, monodentate, and free ionic nitrates present a declining trend after an initial increase, achieving maximum absorbance values for each species of 0.014 (at 6 min), 0.014 (at 6 min), 0.002 (at 8 min), and 0.031 (at 8 min), respectively. During the 16-min observation period, the bands associated with chelating and bridging nitrates decay rapidly, whereas the bands related to free ionic nitrate diminish partly. Therefore, the activity of nitrates is considered to decrease in the order: free ionic nitrates > monodentate nitrates > bridging nitrates > chelating nitrates. Meanwhile, the adsorptions for the gaseous CO_2 band at 2361 and 2336 cm^{-1} are also monitored, and it is found that the signals intensify from 0 to 8 min and then weaken at 10 min (Fig. 5). Hence, it can be concluded that the gaseous CO_2 originated from the oxidation of soot by bridging, chelating, monodentate, and free ionic nitrates.

3.4. Structural characteristics of soot and surface carbon-oxygenated complexes

The structural characteristic of Printex-U soot was examined by XRD. In Fig. 7, the (002) peak at $2\theta = 24.1°$, with a long-term structural order, is due to the stacking structure of graphitic basal planes, while the (10) peak $2\theta = 43.5°$, with a two-dimensional structure, is attributed to graphite-like atomic order within a single plane [15]. The Printex-U soot was exposed to 0.5% NO + 10% O_2/He at 100 °C, and successive DRIFT spectra were recorded at 2-min intervals. As shown in Fig. 7, two major carbon–oxygen functionalities are displayed at 1260 cm^{-1} and

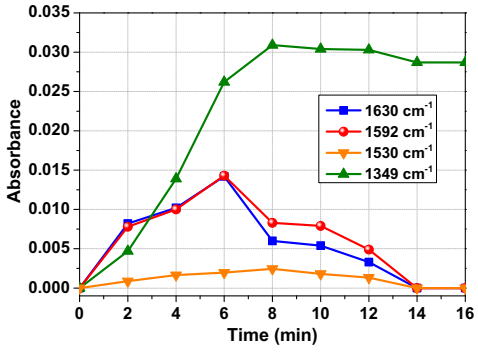

Fig. 6. Absorbance intensity variation of bridging, chelating, monodentate and free ionic nitrates with time.

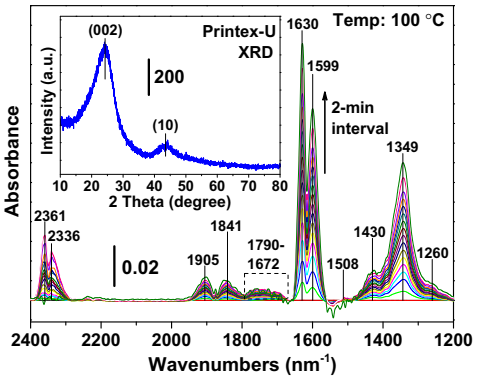

Fig. 7. DRIFT spectra for the Printex-U soot exposed to NO + O_2/He at 100 °C with time. The insert figure is the XRD pattern for Printex-U soot.

1672–1790 cm^{-1} and their intensities are very low owing to the darkness of this soot. Typical wave numbers for carbon–oxygen complexes are summarized in Table 1. The broad absorption between 1672 and 1790 cm^{-1} is assigned to the C═O stretching modes of acidic functional groups such as carboxyls, lactones, and anhydrides. The band at 1260 cm^{-1} is assigned to the absorption of the C—O—C bridge of the anhydride [17]. The prominent adsorption bands at 1349, 1599, and 1630 cm^{-1} are assigned to the free ionic, chelating, and bridging nitrates, reflecting the intense stretching bands of —NO_2. Moreover, the band at 1508 cm^{-1} may arise from the stretching vibrations of monodentate nitrates. The nitrates formed on the carbon surface are dissociative, because they are readily desorbed into the gaseous phase if the sample is flushed with helium [19]. The band at 1430 cm^{-1} is probably attributed to the vibration of NO_2 in C—NO_2. This is because of the fact that the Printex-U soot has distinct graphitic properties as mentioned above. In this case, —NO_2 forms conjugated π-electron systems that are bound via the N atom to aromatic molecules on the graphitic surface edges [20]. At higher wave numbers, the bands at 1841 and 1905 cm^{-1} reflect weakly physisorbed NO. The bands at 2361 and 2336 cm^{-1}, due to CO_2, probably originating from the decomposition of carbon–oxygen functionalities, initially increase with time and then weaken after 19 min. This is consistent with a similar experiment [21], where the combustion product CO_2, released at low temperatures, was attributed to the decomposition of weakly adsorbed CO_x species. After obtaining the information about the adsorbates formed in NO + O_2/He at 100 °C, the sample was heated. In Fig. 8, the adsorptions at 1725,81,736, and 1788 cm^{-1}, assigned to carboxyls, lactones, and anhydrides, respectively, do not show any changes when the temperature is increased to 400 °C [19].

Table 1
DRIFT assignments for surface carbon–oxygen complexes.

Surface carbon–oxygen complexes	Band position (cm^{-1})	Modes	Reference
Quinones	1550–1680	v(C=C)	[16]
Carboxyl	1668–1730	v(C=O)	[18]
Lactone	1675–1790	v(C=C)	[16]
	1745–1765	v(C=O)	[18]
Anhydride	1776–1850	v(C=O)	[18]
	1210–1310	v(C–O)	[18]
Esters	1785–1810	v(C=O)	[17]

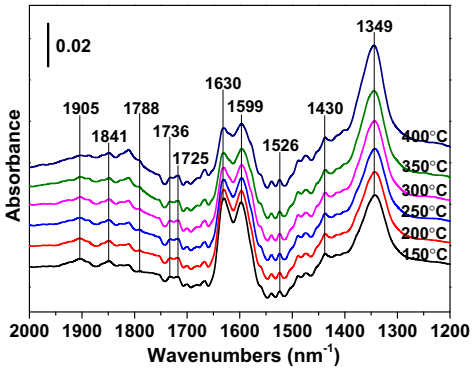

Fig. 8. DRIFT spectra for the Printex-U soot exposed to NO + O_2/He at 150–400 °C.

Similarly, the bands at 1349 cm^{-1} (free ionic nitrates) and 1526 cm^{-1} (monodentate nitrates) are stabile with respect to temperature. However, heating the sample to 400 °C decreases significantly the intensity of the signals at 1599 cm^{-1} (chelating nitrates) and 1630 cm^{-1} (bridging nitrates), which is caused by the desorption of NO_2.

3.5. Surface composition and elemental states of the catalyst

The $La_{0.8}Ce_{0.2}Mn_{0.7}Bi_{0.3}O_3$ catalyst was analyzed by XPS to verify surface composition and elemental states. In Fig. 9A, the XPS signals of Bi 4f at binding energies of 163.9 eV (Bi $4f_{5/2}$) and 158.7 eV (Bi $4f_{7/2}$) over both the fresh and used catalysts are ascribed to Bi^{3+}, which is consistent with the data for Bi_2O_3 powders [22]. Figure 9B shows the spectra of the Mn 2p and Mn 3p XPS region for the catalysts, where the peak at 641.2–641.6 eV arises from Mn $2p_{3/2}$. The distorted Mn $2p_{3/2}$ peak confirms the presence of at least two manganese valence states. However, assignments based on the Mn $2p_{3/2}$ signal are difficult because the separation of the contributions for Mn^{2+}, Mn^{3+}, and Mn^{4+} in oxides is small. Hence, it is standard practice to employ Mn 3p to assign about 47.5 eV for Mn^{2+}, 48.5 eV for Mn^{3+}, and 50.0 eV for Mn^{4+}, respectively, as found for several manganese-based oxides [23]. For the fresh catalyst, the Mn 3p peak at 48.6 eV confirms that the manganese is mostly in a trivalent oxidation state. However, the binding energy value shifts slightly lower (47.9 eV) after oxidation by soot, indicating that part of the Mn^{3+} is reduced to Mn^{2+}. The Ce 3d spectra of the catalysts (Fig. 9C) are individually deconvoluted into $3d_{5/2}$ and $3d_{3/2}$ spin–orbit components (labeled as v and u, respectively) denoting the $Ce^{4+} \leftrightarrow Ce^{3+}$ electronic transitions [24]. The chemical valence of cerium on the fresh catalyst is mainly in the +4 oxidation state (v, v_2, v_3, u, u_2, u_3), but a small quantity of Ce^{3+} (v_1, u_1) also coexists. The O 1s spectra in Fig. 9D display doublet peak profiles, with three discernible components as revealed by a curve fitting analysis. The peak at the highest binding energy (533.1 eV) corresponds to adsorbed molecular water (O_{wat}) while the one at the lowest value (529.1 eV) is associated with lattice oxygen (O_{lat}). The peak located at 531.4 eV corresponds to adsorbed oxygen (O_{ads}) species, such as O^-, O_2^-, and O^{2-}, which are mainly stored on the surface in the form of carbonate, hydroxyl species, and weakly bound oxygen [25].

Table 2 specifies the amount of surface cerium and oxygen species, calculated according to relative peak areas from the respective XPS spectra. The used catalyst possesses a relatively higher O_{lat}/O_{ads} ratio, indicating that the catalyst exhibits higher oxygen mobility during soot oxidation. Moreover, the surface Ce^{3+}/Ce^{4+} atomic ratio for the used catalyst is lower than that of the fresh one. In this case, the increase of Ce^{4+} species together with observation of Mn^{2+} species is indicative of the redox equilibrium ($Mn^{3+} + Ce^{3+} \leftrightarrow Mn^{2+} + Ce^{4+}$) shifting to the right after soot oxidation.

3.6. Proposed reaction pathway

Based on the results discussed above, the catalytic combustion of soot over the $La_{0.8}Ce_{0.2}Mn_{0.7}Bi_{0.3}O_3$ catalyst can be described according to the Langmuir–Hinshelwood mechanism. First, the surface carbon-oxygenated groups are created at free carbon sites, comprising mainly carboxyls, lactones, and anhydrides with good relative thermal stability. The respective bands can be found in the DRIFT spectra at 1725, 1735, and 1788 cm^{-1} (Fig. 8). Considering the exposure of soot to NO + O_2/He at 100 °C, the carbon-oxygenated groups are formed by oxidation of dissociative nitrates rather than by direct O_2. XRD results indicate that the Printex-U soot has a stacking structure of graphitic basal planes and disordered carbon including amorphous carbon and aliphatic

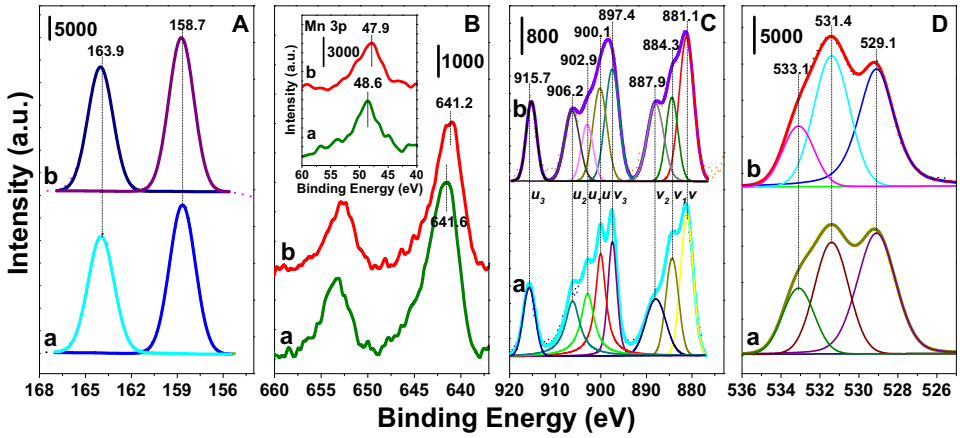

Fig. 9. XPS narrow spectra for Bi 4f (A), Mn 2p and Mn 3p (B), Ce 3d (C), and O 1s (D) for fresh (a) and used (b) $La_{0.8}Ce_{0.2}Mn_{0.7}Bi_{0.3}O_3$ catalysts.

Table 2
Amount of surface cerium and oxygen species from the fresh and used catalysts.

Catalyst	Surface cerium species (at.%)		Ce^{3+}/Ce^{4+}	Surface oxygen species (at.%)			O_{lat}/O_{ads}
	Ce^{3+}	Ce^{4+}		O_{wat}	O_{lat}	O_{ads}	
Fresh	24.2	75.8	0.32	44.6	35.9	19.5	1.84
Used	16.7	83.3	0.20	40.3	42.4	17.3	2.45

side chains that are grafted on the edges of the planes. As such, these carbon-oxygenated groups may cover the inner and outer surfaces of the soot and are located at the edges of graphite platelets or within the section of amorphous carbon.

Second, the adsorption of NO + O_2 on the $La_{0.8}Ce_{0.2}Mn_{0.7}Bi_{0.3}O_3$ catalyst reveals the formation of free ionic, monodentate, chelating, and bridging nitrates on the MnO_x surface, as reflected in the DRIFT spectra at 1349, 1530, 1592, and 1630 cm^{-1}, respectively (Fig. 3). The NO molecule, which has an unpaired electron in its $2\pi^*$ anti-bonding molecular orbital, can exhibit complex adsorption reactions on the manganese surface. NO can adsorb, in two modes, to surface dangling oxygen atoms: first, in a single bond with nitrogen and then with two bonds via the nitrogen and oxygen atoms of the NO molecule to the two surface lattice oxygen atoms [26]. Then, two $-NO_2$ moieties further react disproportionally to produce gaseous NO and an adsorbed $-NO_3$ on the manganese surface. In general, the formation of nitrates on the catalyst surface is considered to be the crucial step affecting the performance of NO_x-soot combustion.

Third, surface activated nitrates exist on manganese sites, with activity decreasing in the order: chelating nitrates > bridging nitrates > monodentate nitrates > free ionic nitrates. These activated nitrates may be released to attack carboxyls, lactones, and anhydrides grafted on the edges of the graphitic planes, accompanied by the reduction of Mn^{3+} to Mn^{2+}. These carbon-oxygenated complexes, such as carboxyls, lactones, and anhydrides, are further oxidized to CO_2, while the nitrates are reduced with release of NO and N_2. After the oxidation of carbon-oxygenated complexes, more free carbon sites will be formed, which will be suitable for adsorbing further oxidizing NO molecules, leading to ring opening and decomposition of the aromatic system via decarboxylation and decarbonylation. Furthermore, three different kinds of adsorbed oxygen species will form at oxygen vacancies on the perovskite surface, namely O^-, O_2^-, and O_2^{2-} [27], which are responsible for $Mn^{2+} \rightarrow Mn^{3+}$ reoxidation. As an oxygen storage material, the cerium oxide has the potential to increase the mass transfer from the gaseous oxygen to the lattice oxygen via the $Ce^{3+} \leftrightarrow Ce^{4+}$ transition.

4. Conclusions

In this study, the NO-soot combustion process over the $La_{0.8}Ce_{0.2}Mn_{0.7}Bi_{0.3}O_3$ catalyst was investigated by in-situ DRIFT, TPO, XPS, and XRD to examine the nature of adsorbed NO_x species and carbon-oxygenated complexes. Soot combustion in a NO + O_2/He atmosphere proceeds via the Langmuir–Hinshelwood mechanism. On the one hand, carbon-oxygenated groups, such as carboxyls, lactones, and anhydrides, are

formed by the oxidation of dissociative nitrates. On the other hand, the adsorption of $NO + O_2$ results in the formation of nitrates on the MnO_x surface of the catalyst. Surface activated nitrates, with activity decreasing in the order: chelating nitrates > bridging nitrates > monodentate nitrates > free ionic nitrates, may further oxidize these carbon-oxygenated complexes with subsequent release of CO_2, NO, and N_2.

Acknowledgments

This study was supported by the National Key Basic Research and Development Program (2013CB228506) and the National Natural Science Foundation of China (No. 51206119).

References

[1] J. Klein, D. Wu, V. Tschamber, I. Fechete, F. Garin, *Appl. Catal. B* 132–133 (2013) 527–534.
[2] F.E. López-Suárez, A. Bueno-López, M.J. Illán-Gómez, *Appl. Catal. B* 84 (2008) 651–658.
[3] E.D. Banús, V.G. Milt, E.E. Miró, M.A. Ulla, *Appl. Catal. A* 362 (2009) 129–138.
[4] X. Guo, M. Meng, F. Dai, et al., *Appl. Catal. B* 142–143 (2013) 278–289.
[5] N. Guillén-Hurtado, A. García-García, A. Bueno-López, *J. Catal.* 299 (2013) 181–187.
[6] W.F. Shuangguan, Y. Teraoka, S. Kagawa, *Appl. Catal. B* 12 (1997) 237–247.
[7] F.E. López-Suárez, S. Parres-Esclapez, A. Bueno-López, M.J. Illán-Gómez, *Appl. Catal. B* 93 (2009) 82–89.
[8] I.S. Pieta, M. García-Diéguez, C. Herrera, M.A. Larrubia, L.J. Alemany, *J. Catal.* 270 (2010) 256–267.
[9] X. Wu, F. Lin, H. Xu, D. Weng, *Appl. Catal. B* 96 (2010) 101–109.
[10] L. Li, X. Shen, P. Wang, X. Meng, F. Song, *Appl. Surf. Sci.* 257 (2011) 9519–9524.
[11] L.Z. Gao, C.T. Au, *Appl. Catal. B* 30 (2001) 35–47.
[12] L. Valencia, R. Bastida, A. Macías, M. Vicente, P. Pérez-Lourido, *New J. Chem.* 29 (2005) 424–426.
[13] W. Shan, F. Liu, H. He, X. Shi, C. Zhang, *Appl. Catal. B: Environ.* 115–116 (2012) 100–106.
[14] A. Sultana, T. Nanba, M. Haneda, H. Hamada, *Catal. Commun.* 10 (2009) 1859–1863.
[15] M. Guerrero, M.P. Ruiz, Á. Millera, M.U. Alzueta, R. Bilbao, *Energy Fuels* 22 (2008) 1275–1284.
[16] J.L. Figueiredo, M.F.R. Pereira, M.M.A. Freitas, J.J.M. Órfão, *Carbon* 37 (1999) 1379–1389.
[17] H. Muckenhuber, H. Grothe, *Carbon* 4 (2007) 321–329.
[18] S. Liu, X. Wu, D. Weng, M. Li, J. Fan, *Appl. Catal. B: Environ.* 138–139 (2013) 199–211.
[19] B. Azambre, S. Collura, J.M. Trichard, J.V. Weber, *Appl. Surf. Sci.* 253 (2006) 2296–2303.
[20] N.B. Colthup, L.H. Daly, S.T.E. Wiberley, Academic Press, New York, 1964.
[21] Z. Zhang, Y. Zhang, Z. Wang, X. Gao, *J. Catal.* 271 (2010) 12–21.
[22] J. Hou, R. Cao, Z. Wang, S. Jiao, H. Zhu, *J. Hazard. Mater.* 217–218 (2012) 177–186.
[23] L. Baggetto, N.J. Dudney, G.M. Veith, *Electrochim. Acta* 90 (2013) 135–147.
[24] F. Zhang, P. Wang, J. Koberstein, S. Khalid, S.W. Chan, *Surf. Sci.* 563 (2004) 74–82.
[25] R.M. Garcia de la Cruz, H. Falcon, M.A. Pena, J.L.G. Fierro, *Appl. Catal. B* 33 (2001) 45–55.
[26] L. Sivachandiran, F. Thevenet, P. Gravejat, A. Rousseau, *Appl. Catal. B* 142–143 (2013) 196–204.
[27] J. Liu, Z. Zhao, C.M. Xu, A.J. Duan, G.Y. Jiang, *J. Phys. Chem. C* 112 (2008) 5930–5941.